POLITECNICO DI TORINO
Repository ISTITUZIONALE

Progress in the analysis of the cavity resonances in the ITER ICRF antenna port plug

*Original*
Progress in the analysis of the cavity resonances in the ITER ICRF antenna port plug / Louche, F., Durodié, F., Kivská, A., Helou, W., Milanesio, D.. - In: EPJ WEB OF CONFERENCES. - ISSN 2100-014X. - ELETTRONICO. - 346:(2026). (25th Topical Conference on Radio-Frequency Power in Plasmas (RFPPC2025) Schloss Hohenkammer (Ger) May 19-22, 2025) [10.1051/epjconf/202634603005].

*Availability:*
This version is available at: 11583/3006642 since: 2026-01-16T11:05:24Z

*Publisher:*
EDP Sciences

*Published*
DOI:10.1051/epjconf/202634603005

*Terms of use:*

This article is made available under terms and conditions as specified in the corresponding bibliographic description in the repository

*Publisher copyright*

(Article begins on next page)

16 November 2026

# Progress in the analysis of the cavity resonances in the ITER ICRF antenna port plug

*Fabrice* Louche[1,*], *Frederic* Durodié[1,], *Alena* Křivská[1,], *Walid* Helou[2,], and *Daniele* Milanesio[3]

[1]Laboratory for Plasma Physics, ERM/KMS, EUROfusion Consortium Member, Brussels, Belgium, TEC Partner
[2]ITER Organization, Route de Vinon-sur-Verdon, CS 90 046, 13067 St. Paul Lez Durance Cedex, France
[3]Politecnico di Torino, Dipartimento di Elettronica, Torino, Italy

**Abstract.** The ITER ICRF antenna plug [1, 2] can exhibit resonances at specific frequencies, some of them in the relevant range of frequencies for IC heating. These resonances have been identified as eigenmodes of the coaxial cavity, where the array plays the role of inner conductor [3], that can substantially increase the level of electric fields within the cavity as well as the level of RF losses. As no grounding solution is considered, RF probes should be installed to monitor the RF fields in the port plug cavity and additional simulations of a realistic magnetized plasma are required to properly assess the integration (position, orientation) and their effectiveness. Several numerical tools are available and have been extensively used to simulate the ITER ICRF antenna, such as TOPICA [5] or CST Microwave Studio (MWS [6]), but none of these codes allow to combine realistic geometries, realistic magnetized plasma profiles, and lossy materials. In this paper we pursue the effort started in [8] where a method based on a modal analysis in the cavity was introduced to decouple solving the computationally intensive plasma facing front of the launcher from the cavity. The method reproduces the TOPICA electric fields (with gyrotropic plasma effects) obtained in a given vertical reference plane, in a MWS cavity (including lossy materials) using the multimodal scattering matrix of the cavity obtained with MWS. This method is here applied to several realistic ITER plasma profiles. The recently extracted magnetic fields [9] from the TOPICA modeling results, provide an alternate way to compute the excitation spectrum of the cavity and therefore allow to confirm our results. Accurate levels of RF losses can then be obtained from various plasma profiles and excitation of the antenna straps.

## 1 Introduction

The ICRF antenna foreseen for ITER consists of an array of 24 short radiating straps grouped in poloidal triplets (4 toroidally and 2 poloidally) through four-port junctions [1]. The system will be operated between 40 and 55 MHz and should deliver 10 MW. It will operate for various toroidal phasings for heating scenarios ($00\pi\pi$, $0\pi0\pi$ and $0\pi\pi0$). Current drive operations in $0\ \pi/2\ \pi\ 3\pi/2$ are also planned. The phase difference between two poloidally adjacent triplets is $-\pi/2$. The most recent status of the RF design of this antenna is reported in [2]. Each antenna is built as a whole assembly inside a port plug that is located within the vacuum vessel, and there is a gap around the antenna between the plug and the vessel. The presence of this gap can induce resonances of the coaxial type: the port plug acts as the inner conductor of a rectangular coaxial line, open on the front side and short-circuited at the back. In particular one of the possible cavity modes occurs in the range of frequency of interest for ICRF: a transverse electric (TE) mode is resonant around 45 MHz and leads to substantially large electric fields in the gap. This effect was observed in 3D numerical simulations [3] and was also validated experimentally with the help of a reduced-scale mock-up of the antenna [4]. As soon as the effect was identified, it was first considered to develop a grounding of the antenna plug in such a way to reduce the electrical length of the cavity and move the resonance out of the ICRF range [3, 4]. But mechanical considerations made these grounding solutions unpractical and unacceptable, and various strategies were considered. Among those, there is the option to monitor the RF fields in the cavity with the help of RF probes.

An accurate evaluation of the RF electric fields and currents is required to precisely define the location and the orientation of the RF probes in case the latter are used, and therefore a consistent modeling of the precise geometry of the antenna front face, of the cavity, including the various lossy materials, and of the magnetised plasma for realistic plasma density profiles is required. A layer of Boron Carbide ($B_4C$) to absorb the incoming neutrons will notably be present at the back of the cavity, and an accurate assessment of the RF losses in the material is required[1]. Various numerical codes are available and were used during the last couple of decades to model the ITER antenna. Among those, TOPICA [5], on the one hand, is a plasma coupling code that allows for realistic plasma profiles and can simu-

*Corresponding author: fabrice.louche@rma.ac.be

[1]At the time of the present study blank $B_4C$ tiles were considered in ITER. In the meantime they could be enclosed in a metallic box.

© The Authors, published by EDP Sciences. This is an open access article distributed under the terms of the Creative Commons Attribution License 4.0 (https://creativecommons.org/licenses/by/4.0/).

late a detailed model of the ITER antenna including a PEC (Perfectly Electric Conducting) cavity. A limitation of the code is the impossibility to properly represent lossy materials, a requirement to compute accurate values of the RF losses in the cavity. On the other hand, the 3D electromagnetic commercial software CST Microwave Studio® (MWS [6]) either uses the approximation of a dielectric loading to emulate a plasma, or a cold magnetised plasma dielectric tensor, but continuously varying spatial profiles cannot be properly simulated. Only stratified profiles are possible [7], and this comes at the price of additional numerical complexity.

In [8] we proposed to decouple solving the computationally intensive plasma facing front of the launcher from the cavity. The idea is to import the RF fields and currents from TOPICA evaluated in a given vertical plane and for a given cavity, and to reproduce them in the same plane in the MWS cavity by expanding them in cavity eigenmodes. We present here the results of this analysis for three reference ITER plasma density profiles.

## 2 Modal analysis: methodology

Figure 1 shows the 3D RF electric field computed by TOPICA at 47.5 MHz for the "LowCut" plasma profile, in $0\pi\pi0$ toroidal phasing. Note that the poloidal phasing is $-\pi/2$ for all the simulations presented here, and the fields are normalized to a 45 kVmaximum voltage in the transmission lines. We also show the variation of the field amplitude along a reference curve centred in the gap. The curve starts from the centre of the bottom gap and loops counterclockwise around the inner conductor, see Figure 2(a).

As a first step, we expand the transverse component $\mathbf{E_{RF}}$ in a series of cavity eigen-modes:

$$\mathbf{E_{RF}} = \sum_n A_n \widehat{\mathbf{e_n}} \tag{1}$$

with

$$A_n \simeq \oint g(s) E_{RF,\xi}(s) e^*_{n,\xi}(s) ds \ . \tag{2}$$

where $s$ is the coordinate along the curve, $g(s)$ is the length of the local normal gap, $e_{n,\xi}(s)$ are the normal components (with respect to the curve) of the eigen-modes which satisfy $\oint g(s) e_{m,\xi} e^*_{n,\xi} ds = \delta_{mn}$ [8], see Figure 2(b). The approximated relation (2) is valid as long as the ratio of the gap width to the gap circumference is small, therefore the fields of the TEM and TE modes are relatively constant across the gap width. In practice the sum (1) is limited to *nmax* terms. The first eigenmode is the first TEM mode, while the other modes are TE modes that are ordered according to their increasing respective cut-off frequency. Figure 3 shows the profile of the first four modes along the reference curve.

The tangential RF magnetic fields $\mathbf{H_{RF}}$ were recently extracted from the TOPICA outputs [9]: they are evaluated along a curve tangent to the inner conductor of the cavity, and they can also be expanded in series of eigen-modes:

$$\mathbf{H_{RF}} = \sum_n B_n \widehat{\mathbf{h_n}} \tag{3}$$

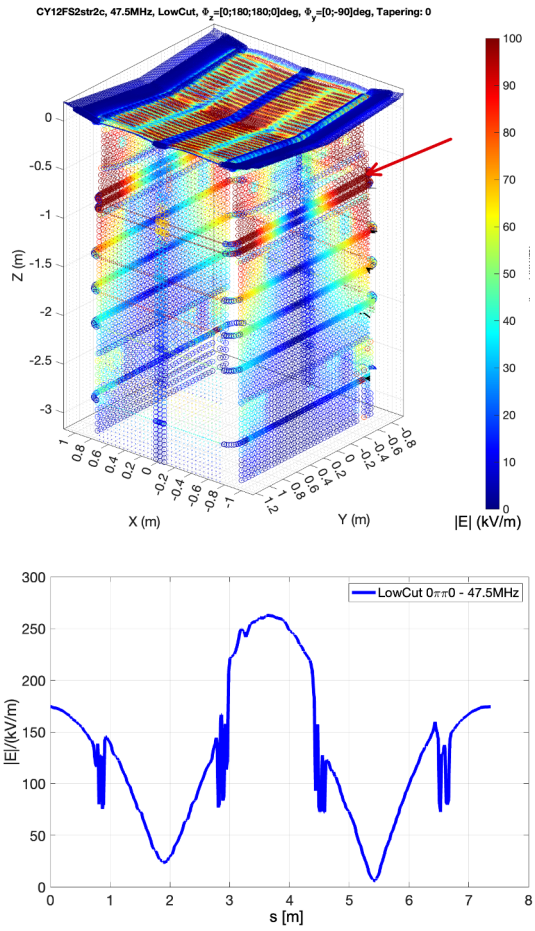


**Figure 1.** Top: RF electric field from TOPICA, "LowCut" plasma profile, 47.5 MHz - $0\pi\pi0$ - the thick arrow shows the vertical plane where the fields are measured; bottom: amplitude of the same electric field along the reference curve in the gap, in the vertical plane indicated by the arrow.

with

$$B_n = (Z_n)^2 \iint_S \mathbf{H_{RF}} \widehat{\mathbf{h_n}}^* dS \simeq (Z_n)^2 \oint g(s) H_{RF}(s) h^*_n(s) ds. \tag{4}$$

$Z_n$ being the wave impedance of mode $n$. The magnetic eigen-modes satisfy the orthonormality relation $\iint_S \widehat{\mathbf{h_n}} \widehat{\mathbf{h_m}}^* dS = (Z_n)^{-2} \delta_{mn}$. The values of $Z_n$ at 47.5 MHz for the first 10 modes are given in Table 1.

**Table 1.** Wave impedance in ohms of the first 10 eigen-modes at 47.5 MHz.

| Mode # | 1 | 2 | 3 | 4 | 5 |
|---|---|---|---|---|---|
| $Z_n$ [Ω] | 376.7 | 711.5 | 746.3 | $273.1j$ | $266.8j$ |
| Mode # | 6 | 7 | 8 | 9 | 10 |
| $Z_n$ [Ω] | $159.4j$ | $159.2j$ | $115.5j$ | $114j$ | $90.8j$ |

With the knowledge of the modal content $\mathbf{A} = (A_1, ..., A_n, ..., A_{nmax})$ and $\mathbf{B} = (B_1, ..., B_n, ..., B_{nmax})$ of the TOPICA electric and magnetic fields respectively, we want to know which spectrum of the incoming eigen-

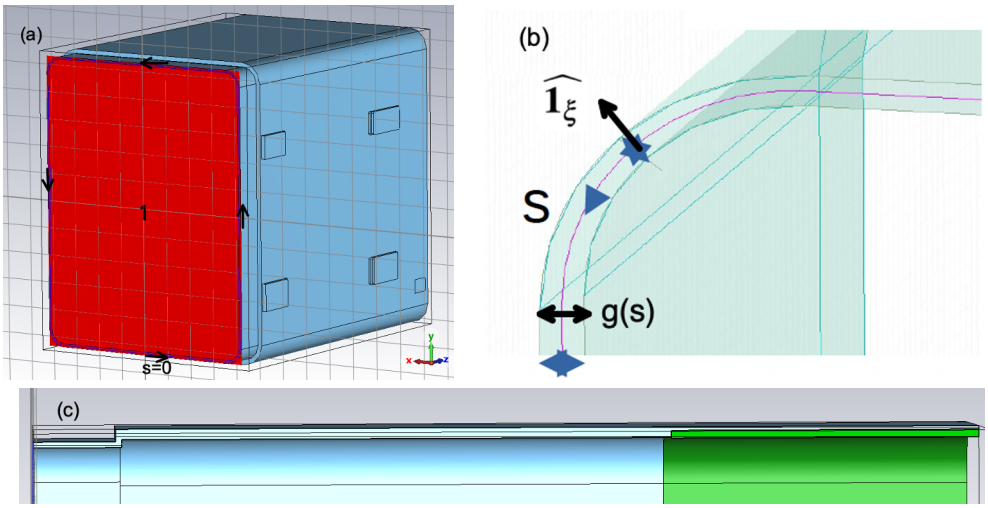


**Figure 2.** Cavity model in MWS. (a): front view of the inner vacuum volume of the cavity, with the port where the excitation spectrum is defined in red, and the cartesian reference frame; the origin and counter-clockwise direction of the curves are also visible; (b): zoom on the central curve where the electric fields are evaluated, with the definition of the length parameter $s$, the local gap $g(s)$, and the normal unit vector $\widehat{\mathbf{1}}_\xi$; (c) vertical cut view of the top of the cavity; the volume in green is the lossy $B_4C$.

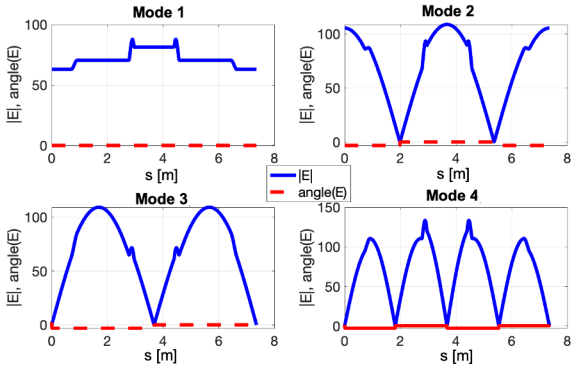


**Figure 3.** First four eigen-modes of the rectangular cavity: magnitude of the electric field along the reference curve.

modes will reproduce the TOPICA field in the MWS cavity, this field being the sum of an incoming field and a reflected field. The first method only involves the electric field modal content **A**. If we define the vector $\alpha$ as the excitation of the incoming eigen-modes at the port (see Figure 2(a)), $E^{(+)} = \Sigma_n \alpha_n \widehat{\mathbf{e}}_\mathbf{n}$, we have [8]

$$\alpha = (\mathbf{S} + \mathbf{I})^{-1}\, \mathbf{A}\ , \tag{5}$$

where **S** is the multi-modal scattering matrix that connects the incident and reflected waves for each eigen-mode excitation of the cavity, **I** is the unity square matrix of order *nmax*. Another method uses the electric and the magnetic field modal contents [10]:

$$\alpha = \frac{1}{2}\,(\mathbf{A} + \mathbf{B})\ . \tag{6}$$

The solutions (5) and (6) are formally equivalent, but in practice the accuracy with which MWS computes the scattering matrix will depend on the way the evanescent eigen-modes are numerically treated by the code. It should be reminded that only the first three modes are propagative at the frequency of concern and that all the superior modes are below their cut-off. To ensure that the electromagnetic properties of the metallic cavity used in TOPICA are the same as the lossy cavity in CST, we have checked that the matrix of the lossy cavity does not change when the losses are neglected, as not only geometrical inhomogeneities, but also material changes could induce superior modes excitations and mode couplings. We have considered a relative electric permittivity of 4.8 and a conductivity of 1000 S/m for the lossy material $B_4C$. Figure 4 the absolute value of the multimodal scattering matrix for the first 15 modes. If some cross-coupling are observed, they are due to the existence of sharp geometry transitions ("dog-legs", see Figure 2(c)) along the axis of the cavity. It appears that the presence of the lossy layer has a negligible influence.

## 3 Modal analysis: results

We first consider the expansion of the TOPICA fields evaluated along the respective curves in eigen-modes, (1) and (3): we have evaluated the coefficients $A_n$, defined by (2), and $B_n$, defined by (4), respectively. We considered the reference profile "LowCut" and the various toroidal phasings considered for heating: $00\pi\pi$, $0\pi0\pi$, $0\pi\pi0$, as well as monopole 0000 (not really a heating scenario but useful to assess a "worst case scenario"). A typical property of the first two phasing cases is the presence of a vertical electric symmetry plane, characterized by a zero $y$ component of the electric field and maximum $H_y$ and $H_z$, while the two latter cases exhibit a vertical magnetic symmetry plane (with maximum $E_y$ and zero $H_y$ and $H_z$). The cartesian reference frame is visible in Figure 2(a). It is therefore expected that the eigen-modes preferentially excited for each case will exhibit the same symmetry properties in their components. This is what was observed previously in [8] is confirmed in the top plots of Figure 5. The mode

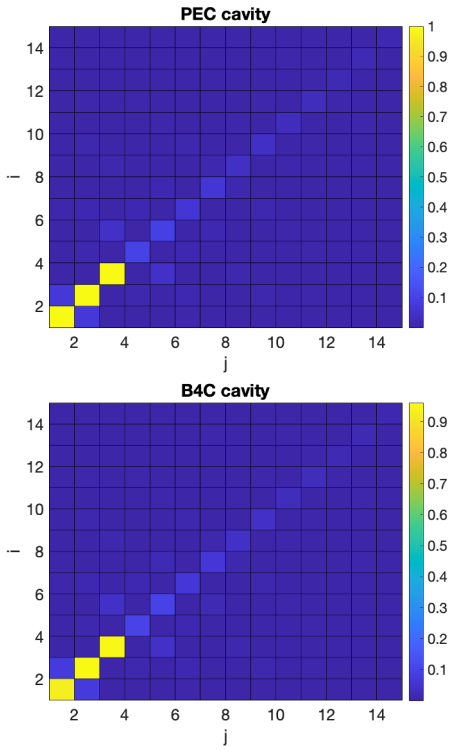


**Figure 4.** First elements of the multimodal scattering matrix $S_{ij}$ (absolute value) for various material assumptions of the rectangular coaxial cavity: top: metallic cavity; bottom: cavity with $B_4C$ layer.

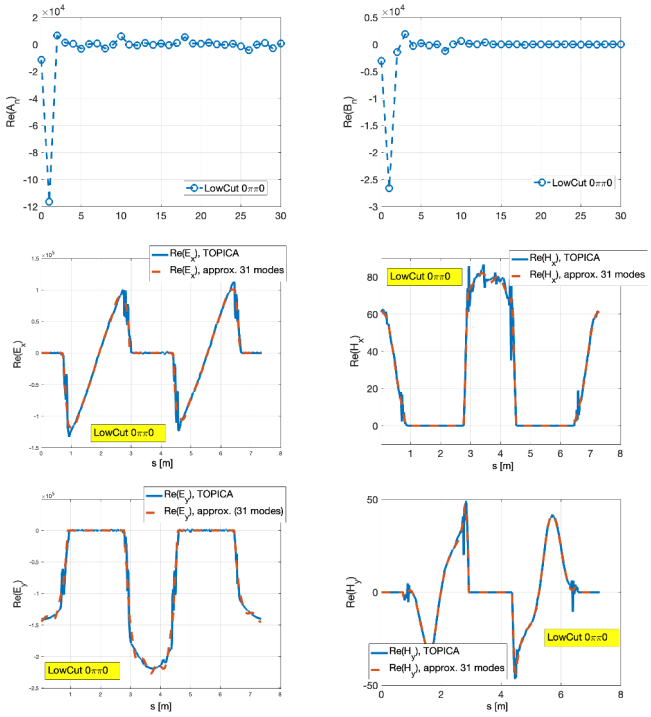


**Figure 5.** Case of "LowCut" plasma profile, at f = 47.5 MHz and $0\pi\pi0$ toroidal phasing: real parts of the normal electric field (left) and tangential magnetic field (right). Top: modal content. Centre: $x$-component of the fields: TOPICA solution and expansion limited to 31 modes. Bottom: $y$-component of the fields: TOPICA solution and expansion limited to 31 modes.

principally excited is the $TE_{1a}$ mode characterized by a peak in $E_y$ and $H_x$ in the vertical midplane. We also plotted on the same figure he original TOPICA fields compared with the expansions (1) and (3) limited to 31 modes: we see that the TOPICA fields along the curve are perfectly reproduced. The larger gap width in the bottom part of the cavity (25mm) as compared with the top (15mm) explains the different amplitudes of the maxima. The displayed pictures show the results for the real part of the fields, the imaginary parts behave in the same way in terms of modal content and accuracy of the TOPICA fields reconstruction.

We did the same exercise with the $00\pi\pi$ toroidal phasing: see Figure 6. We observe a dominant excitation of mode $TE_{1b}$ for the electric field, as expected. However, unlike the previous case where the maxima of the electric field were well toroidally centred in the top/bottom gaps, the maxima located in the side gaps are strongly displaced with respect to the horizontal mid-plane, showing that the field distribution is affected by the poloidal phasing difference of $-\pi/2$ between the top and bottom half-arrays. This is why superior modes $TE_{2b}$ and $TE_{3b}$ contribute significantly to the expansion. This is particularly visible for the magnetic field. We also see a perfect reproduction the TOPICA field with the expansion limited to a reasonable number of modes.

We were able to compute the modal content of the TOPICA electric and magnetic fields for the various configurations plasma profile/toroidal phasing, i.e. the contents of the vectors **A** and **B**. In the next section we will compute the corresponding spectra of excitation which reproduce the TOPICA fields in the MWS cavity.

## 4 Modal excitation of the cavity

In section 2 we introduced two formulations of the excitation spectrum vector $\alpha$, equations (5) and (6), which we respectively label "*Smat*" and "*EH*". The electric field incident to the port of the MWS cavity is therefore defined as

$$E^{(+)} = \Sigma_n \alpha_n \widehat{\mathbf{e}_\mathbf{n}} \,, \tag{7}$$

and the resulting total electric field can be obtained from MWS, as well as local RF electric fields, RF currents in the cavity, and by consequent integrated volume RF losses.

Figure 7 shows the $x$-component of the total electric and magnetic fields obtained following the two formulations, superposed on the actual TOPICA fields, for the three phasings. The general impression is that for the electric fields the total reconstructed fields are in very good agreement with the TOPICA fields, for both methods. As far as the magnetic field is concerned, we observe significant discrepancies in $0\pi\pi0$ phasing in the bottom part of the cavity, where the maxima are clearly underestimated. In $0\pi0\pi$, only the "*EH*" method is able to correctly reproduce the variations of the magnetic field. "*Smat*" completely misses the strong change of sign at the top of the cavity. This is probably due to an inaccurate treatment of

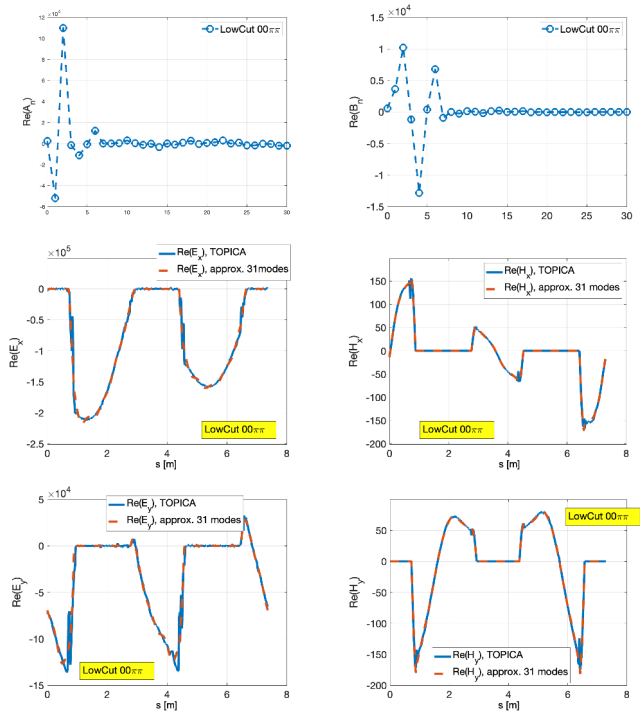


**Figure 6.** Case of "LowCut" plasma profile, at f = 47.5 MHz and $00\pi\pi$ toroidal phasing: real parts of the normal electric field (left) and tangential magnetic field (right). Top: modal content. Centre: $x$-component of the fields: TOPICA solution and expansion limited to 31 modes. Bottom: $y$-component of the fields: TOPICA solution and expansion limited to 31 modes.

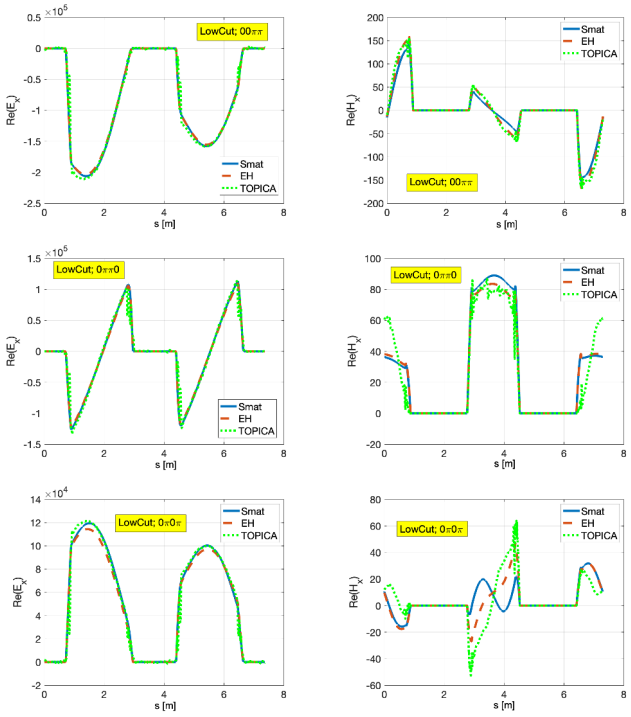


**Figure 7.** Total cavity electric and magnetic fields ($x$-component, real part) at 47.5 MHz along the $s$-curves in the MWS cavity: comparison between the fields reproduced by the "*Smat*" and "*EH*" methods ((5) and (6) respectively) and the TOPICA field, for the reference heating toroidal phasings.

the evanescent superior modes by MWS, as we know that this phasing needs non-negligible contributions from these modes to be properly described. The effect is also visible in $00\pi\pi$, where the inflexion point and the change of concavity of $Re\,(H_x(s))$ at the center of the top gap are not properly described. Also for this latter case the method (6) gives a better result. These plots were produced with 11 modes in the expansion, but increasing the number of modes does not make the solution more accurate.

We have been able to reproduce the TOPICA fields in the MWS cavity with a satisfactory level of accuracy, and for the following discussion we will use the results provided by the "*EH*" method. The distribution of the field amplitude is plotted in Figure 8: this will allow to precisely determine the best position of the RF probes during ITER first phase of ICRH operation. It should be reminded that these fields were computed with the assumption of a maximum voltage of 45kV in the transmission lines. From these fields we can compute the expected level of RF losses in the $B_4C$ layer under the same assumption. For all the considered cases where the coupled power $P_C$ is larger than the maximum power of 10MW available from the source, we have renormalized the RF losses $P_L$ and the maximum local electric field magnitude $E_{max}$ for a maximum coupled power of 10MW, see Table 4. Interestingly, the trends and the orders of magnitude of the RF losses are very similar to what was presented in [11], where preliminary evaluations of the RF losses and fields at the resonance were performed in MWS with an equivalent dielectric loading and a simplified geometry of the antenna. The "LowCut+150cm" case is equivalent to a vacuum loading, and is presented as an illustration, stressing the strong impact of very low coupling situations on the excitation of the resonance. In wall conditioning scenarios it is clear that there is some freedom in the choice of the generator frequency and it is very likely that the resonance regime will be avoided.

## 5 Conclusion

The problem of the excitation of cavity resonances between the ITER ICRF antenna and the ICRF port plug was identified in [3] but it became clear that no grounding solution could be technically considered. Therefore, a thorough evaluation of the potential consequence of these modes on the operation of the antenna was deemed necessary. The numerical tools available do not individually allow to assess the level of RF fields in the cavity with a detailed geometry of the array and of the cavity, and a realistic description of the magnetised plasma and the lossy materials. In [8] a method that can combine the various approaches was proposed. It allows to include a detailed geometry of the antenna, the gyrotropic effects induced by the magnetised plasma, and the lossy materials. In the present work we extended the method and used it on a series of results (RF electric fields and surface currents) from TOPICA modelings, with various toroidal phasings and

**Table 2.** Cavity RF electric fields & RF losses (assuming uncoated $B_4C$)

| Profile | Phasing | $P_C$/MW | $P_L$/kW | | $E_{max}$/(kV/m) | |
|---|---|---|---|---|---|---|
| | | 45 kV max. | 45 kV max. | 10 MW max. | 45 kV max. | 10 MW max. |
| "LowCut" | $00\pi\pi$ | 15.3 | 40 | 26.1 | 33.8 | 27.3 |
| "LowCut" | $0\pi\pi0$ | 11.1 | 43 | 38.7 | 36.4 | 34.5 |
| "LowCut" | $0\pi0\pi$ | 9.1 | 33.5 | - | 28.9 | - |
| "LowCut-4cm" | $00\pi\pi$ | 24.6 | 28 | 11.4 | 31 | 19.8 |
| "LowCut-4cm" | $0\pi\pi0$ | 19.7 | 11 | 5.6 | 19.1 | 13.6 |
| "LowCut-4cm" | $0\pi0\pi$ | 17.4 | 12 | 6.9 | 17.7 | 13.4 |
| "LowCut+150cm" | 0000 | - | 1600 | - | 2215 | - |

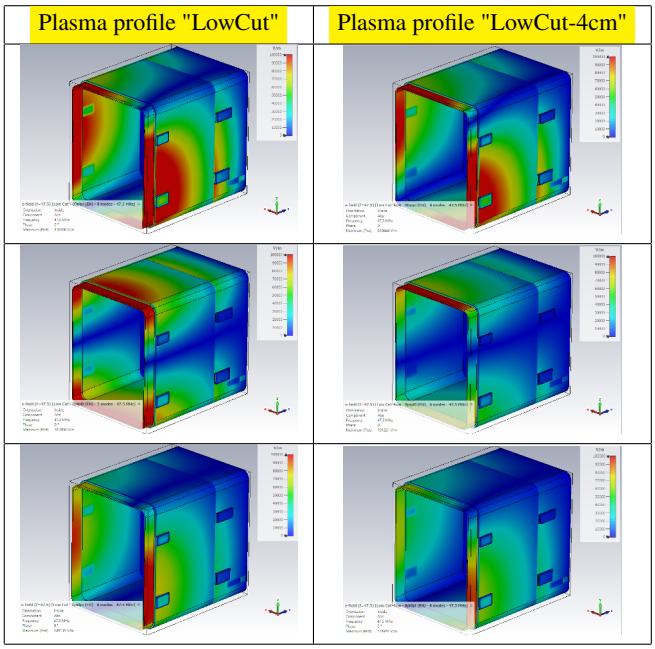


**Figure 8.** 3D electric fields amplitude distribution in the MWS cavity (45 kV max. in the transmission lines) for two plasma profiles and three cases of toroidal phasings (from top to bottom): $00\pi\pi$, $0\pi\pi0$ and $0\pi0\pi$. Plots maximum is 100 kV/m.

plasma profiles. From the evaluation of the model content of these fields and the subsequent calculation of the modal excitations of the cavity, we could not only reproduce the TOPICA fields in a model of the cavity in CST MWS, but from this we were able to evaluate the maximum fields expected in the cavity, as well as the RF losses.

This information will guide the next steps in the planification of ICRF in ITER. A procedure will indeed have to be defined to avoid the regime where the resonance appears during the operation of the antenna. At the time of writing there is still no final decision about the strategy involving the RF probes: location, calibration, how long they will stay and whether they will be kept installed during operation in the tokamak. In case no probes are considered, another option would involve the measurement of the scattering matrix at the back of the 8 four-port junctions and the identification of the peaks where the resonances occur.

## 6 Disclaimer

The views and opinions expressed herein do not necessarily reflect those of the ITER Organization.

## References

[1] B. Beaumont et al., Status of the ITER Ion Cyclotron H&CD. EPJ Web of Conferences **157**, 02002 (2017) https://doi.org/10.1051/epjconf/201715702002

[2] W. Helou et al., The ITER ICRF System Under the New ITER baseline: Latest Updates and Technological Developments. 25th Topical Conference on Radio-Frequency Power in Plasmas, Schloss Hohenkammer, Germany, May 19-22 (2025). https://www.ipp.mpg.de/5487515/Talks

[3] F. Louche et al., Eigenmode analysis of the ITER ICRF antenna plug and electrical solution to the grounding of the antenna, Nucl. Fusion **49**, 065025 (2009) https://doi.org/10.1088/0029-5515/49/6/065025

[4] P. Dumortier et al., ITER ICRH antenna grounding options, Fusion Engineering and Design **88**, 922–925 (2013) https://doi.org/10.1016/j.fusengdes.2013.01.005

[5] V. Lancelotti et al., TOPICA: an Accurate and Efficient Numerical Tool for analysis and design of ICRH antennas, Nucl. Fusion **46**, S476 (2006). https://doi.org/10.1088/0029-5515/46/7/S10

[6] CST Studio Suite 2025, https://www.3ds.com/products/simulia/electromagnetic-simulation

[7] F. Louche et al., Simulation of cold magnetized plasmas with the 3D electromagnetic software CST Microwave Studio®, EPJ Web of Conferences **145**, (2017), https://doi.org/10.1051/epjconf/201715703031

[8] F. Louche et al., Modal analysis of the fields in the ITER ICRF antenna port plug cavity, AIP Conf. Proc., **2984**, 060007 (2023). https://doi.org/10.1063/5.0162511

[9] A. Křivská et al, Estimation of the magnetic field and its modal analysis in the port plug cavity of the ITER antenna, 25th Topical Conference on Radio-Frequency Power in Plasmas, Schloss Hohenkammer, Germany, May 19-22 (2025).

[10] John David Jackson, Classical Electrodynamics, 3rd Ed., (John Wiley & Sons 389–392, 1999)

[11] F. Louche, Simulation for the cavity modes, Report on Task1.a, IO contract IO/20/CT4300002178 (2021)